

Title

Identification of *IGF2* as Genomic Driver and Actionable Therapeutic Target in Hepatoblastoma

Authors

Jordi Abril-Fornaguera^{1,2*}, Laura Torrens^{1,2*}, Carmen Andreu-Oller^{1,2*}, Juan Carrillo-Reixach³, Alex Rialdi¹, Ugne Balaseviciute², Roser Pinyol², Carla Montironi^{1,2}, Philipp K. Haber¹, Álvaro Del Río-Álvarez³, Montserrat Domingo-Sàbat³, Laura Royo³, Nicholas K. Akers^{1,4}, Catherine E. Willoughby², Judit Peix², Miguel Torres-Martin^{1,2}, Marc Puigvehi^{1,5}, Stefano Cairo⁶, Margaret Childs⁷, Rudolf Maibach⁸, Rita Alaggio⁹, Piotr Czauderna¹⁰, Bruce Morland¹¹, Bojan Losic^{1,4}, Vincenzo Mazzaferro¹², Ernesto Guccione¹, Daniela Sia¹, Carolina Armengol^{3,13,14,#}, Josep M. Llovet^{1,2,15,#}

* These authors contributed equally to this work.

These authors contributed equally to this work.

Author affiliations

1. Mount Sinai Liver Cancer Program, Division of Liver Diseases, Tisch Cancer Institute, Icahn School of Medicine at Mount Sinai, New York, USA.
2. Translational Research in Hepatic Oncology Group, Institut d'Investigacions Biomèdiques August Pi i Sunyer (IDIBAPS), Hospital Clínic, Universitat de Barcelona, Barcelona, Catalonia, Spain.
3. Childhood Liver Oncology Group (c-LOG), Health Sciences Research Institute Germans Trias i Pujol (IGTP), Badalona, Catalonia, Spain.
4. Department of Genetics and Genomic Sciences, The Icahn Institute for Genomics and Multiscale Biology, Icahn School of Medicine at Mount Sinai, New York, USA.
5. Hepatology Section, Gastroenterology Department, Parc de Salut Mar, Hospital del Mar Medical Research Institute (IMIM), Barcelona, Catalonia, Spain.

- 31 6. XenTech, Evry, France.
- 32 7. Nottingham Clinical Trials Unit, Nottingham, United Kingdom.
- 33 8. International Breast Cancer Study Group Coordinating Center, Bern, Switzerland.
- 34 9. Pathology Unit, Bambino Gesù Children's Hospital, IRCCS, Rome, Italy.
- 35 10. Department of Surgery and Urology for Children and Adolescents, Medical
- 36 University of Gdansk, Gdansk, Poland.
- 37 11. Department of Oncology, Birmingham Women's and Children's Hospital,
- 38 Birmingham, United Kingdom.
- 39 12. Fondazione IRCCS Istituto Nazionale dei Tumori, Milan, Italy.
- 40 13. Liver and Digestive Diseases Networking Biomedical Research Centre (CIBEREHD),
- 41 Madrid, Spain.
- 42 14. Program for Predictive and Personalized Medicine of Cancer (PMPPC), Health
- 43 Sciences Research Institute Germans Trias i Pujol (IGTP), Badalona, Catalonia,
- 44 Spain.
- 45 15. Institutió Catalana de Recerca i Estudis Avançats, Barcelona, Catalonia, Spain.

46

47 **Running title**

48 *IGF2* is a driver and an actionable target in hepatoblastoma

49

50 **Corresponding authors**

51 [#]Josep M. Llovet, MD, PhD; ORCID: 0000-0003-0547-2667. Address: Liver Cancer
 52 Translational Research Laboratory, Liver Unit, IDIBAPS-Clinic Barcelona, University of
 53 Barcelona, Rosselló 153, 08039, Barcelona, Catalonia, Spain; Tel.: +34 932 279 155;
 54 Email address: jmllovet@recerca.clinic.cat

55 [#]Carolina Armengol, MD; ORCID: 0000-0002-4690-4027. Address: Childhood Liver
 56 Oncology Group (c-LOG), Germans Trias i Pujol Research Institute (IGTP), Edifici
 57 Muntanya, Campus Can Ruti, Ctra. de Can Ruti. Camí de les Escoles, s/n 08916
 58 Badalona, Spain. Tel.: + 34 935 543 072, E-mail address: carmengol@igtp.cat

59

60 **Authors' Disclosures**

61 This study was supported by a research grant from Boehringer Ingelheim. JML is
 62 receiving research support from Bayer HealthCare Pharmaceuticals, Eisai Inc, Ipsen,

63 Boehringer-Ingelheim and consulting fees from Eli Lilly, Bayer HealthCare
64 Pharmaceuticals, Eisai Inc, Merck, Bristol-Myers Squibb, Ipsen, Glycotest, Nucleix,
65 Genentech, Roche, and AstraZeneca. The remaining authors declare no competing
66 interests.

67

68 ABSTRACT

69 Management of hepatoblastoma (HB), the most frequent pediatric liver cancer, is
70 based on surgical resection and perioperative chemotherapy regimens. In this study,
71 we aimed to identify actionable targets in HB and assess the efficacy of molecular
72 therapies in preclinical models of HB.

73 Paired tumor and adjacent tissues from 31 HBs and a validation set of 50 HBs were
74 analyzed using RNA-seq, SNP and methylation arrays. *IGF2* overexpression was
75 identified as the top targetable HB driver, present in 71% of HBs (22/31). *IGF2*^{high}
76 tumors displayed progenitor cell features and shorter recurrence-free survival. *IGF2*
77 overexpression was associated in 91% of cases with fetal promoter hypomethylation,
78 ICR1 deregulation, 11p15.5 loss of heterozygosity or miR483-5p overexpression.

79 The antitumor effect of xentuzumab (a monoclonal antibody targeting IGF1/2) alone or
80 in combination with the conventional therapeutic agent cisplatin was assessed in HB
81 cell lines, in PDX-derived HB organoids and in a xenograft HB murine model. The
82 combination of xentuzumab with cisplatin showed strong synergistic antitumor effects
83 in organoids and in *IGF2*^{high} cell lines. In mice (n=55), the combination induced a
84 significant decrease in tumor volume and improved survival compared to cisplatin
85 alone.

86 These results suggest that *IGF2* is an HB actionable driver and that, in preclinical
87 models of HB, the combination of IGF1/2 inhibition with cisplatin induces superior
88 antitumor effects than cisplatin monotherapy. Overall, our study provides a rationale
89 for testing *IGF2* inhibitors in combination with cisplatin in HB patients with *IGF2*
90 overexpression.

91 INTRODUCTION

92 Hepatoblastoma (HB) is the most common pediatric liver cancer, generally occurring in
 93 children under 3 years of age[1]. Although its incidence has substantially increased
 94 over the last 30 years, HB is a rare disease, with 1.8 cases per million children/year[2,
 95 3]. Unlike hepatocellular carcinoma (HCC), the most common primary liver tumor in
 96 adults, HB develops in the absence of an underlying liver disease or viral etiology. Most
 97 HB tumors occur sporadically, and only 5% of cases are associated with genetic
 98 diseases such as Beckwith-Wiedemann syndrome or Familial adenomatous
 99 polyposis[4].

100 Despite adjuvant and neoadjuvant cisplatin-based chemotherapy improves clinical
 101 outcome after resection[5], recurrence-free survival at 3 years for patients with
 102 advanced stages is only of 34%[6]. Furthermore, chemotherapy regimens are
 103 associated with severe and lifelong side effects such as ototoxicity and
 104 cardiomyopathy[7], which have especially impactful consequences for patients who
 105 are treated at early ages. Considering this, new treatment strategies are urgently
 106 awaited, and the identification of novel actionable drivers in HB is a current unmet
 107 medical need.

108 HB is a heterogeneous disease, so a better understanding of the molecular features of
 109 HB tumors is a prerequisite for developing targeted therapies. In this line, new HB
 110 classifications are emerging and include the so-called hepatocellular neoplasms not
 111 otherwise specified (HCN-NOS)[8, 9]. Globally, HBs present one of the lowest somatic
 112 mutation rates of all cancer types[10, 11], being mutations or deletions in the gene
 113 encoding β -catenin (*CTNNB1*) the most recurrent alteration (70-80% of HB
 114 patients)[12, 13], followed by mutations in *NFE2L2* (10%) or in the *TERT* promoter
 115 (6%)[10], the latter mainly representing HCN-NOS cases[9]. On the other hand, Insulin
 116 Like Growth Factor 2 (*IGF2*) overexpression in HB has been proposed as a potential
 117 oncogenic driver[14, 15]. In HCC, IGF signaling has been identified as an epigenetic
 118 driver[16, 17] and has shown great promise as an actionable target in preclinical HCC
 119 experimental models[18]. Sensitivity of HB cells to IGF1R/IGF2 pathway inhibition has
 120 been demonstrated *in vitro*[15]. In the clinical context, IGF2 inhibition with
 121 xentuzumab (BI 836845; see ref. [19] for full sequence and structure), a monoclonal
 122 antibody against IGF1 and IGF2, is under investigation in different tumor types

(NCT02191891, NCT03659136, NCT03099174, NCT02123823 and NCT02204072). In this regard, preliminary results of phase 1 trials have revealed that xentuzumab has promising antitumor activity and is well tolerated[20]. However, its clinical efficacy and safety in children with HB have not yet been explored.

Here, we analyzed 31 HB tumors, including HB (n=29) and HCN-NOS (n=2), and identified IGF2 as the main targetable deregulated pathway in HB. We then showed that IGF2^{high} HBs are associated with poor outcome, which was the basis for testing xentuzumab alone or in combination with cisplatin –the backbone of all neoadjuvant chemotherapies in HB patients and the standard of care for standard-risk HB– in HB cell lines, in a PDX (patient derived xenograft)-derived tumor organoid model and in a xenograft murine model mimicking IGF2^{high} HBs. *In vitro*, the combination exerted a synergistic reduction in viability and, *in vivo*, it improved survival and inhibited tumor angiogenesis compared to cisplatin. Overall, our findings suggest that HB patients with high IGF2 levels could benefit from xentuzumab combined with chemotherapy, and are a first step towards the implementation of precision medicine in HB.

138

139 MATERIALS AND METHODS

140

141 *Human HB cohorts*

The study cohort included primary HB tumor and adjacent non-tumor samples obtained from 31 patients[21] who received resection after standard neo-adjuvant therapy. Data from RNA sequencing, methylation array, SNP-array and human transcriptomic array data (GSE132219) have been previously reported elsewhere[21] (Supplementary Figure 1). The patient's clinicopathological data are summarized in Table 1. As validation cohort, we used an in-house cohort of 50 HB tumors and 2 non-tumor formalin-fixed paraffin-embedded (FFPE) tissue samples from patients enrolled in the SIOPEL-3 clinical trial[22]. A second validation cohort consisting of published RNA sequencing data (GSE104766) from 25 HB tumors and their respective non-tumor adjacent tissue was used[23]. All samples were collected in accordance with European and Spanish law. Informed written consent was obtained from each patient in accordance with European guidelines for biomedical research. The study conformed to the ethical guidelines of the 1975 Declaration of Helsinki, and it was approved by the

Human Ethics Committee of the Hospital Universitari Germans Trias i Pujol. All samples were histologically reviewed by two expert liver pathologists (R.A. and C.G.).

Transcriptomic analysis

RNA-seq data from 31 HB tumor and adjacent non-tumor pairs from the study cohort[21] was used. Raw expression counts were normalized with the weighted “trimmed mean method” (TMM) implemented in the edgeR package[24] to correct library size differences between samples. The gene expression profile in HB tumors was analyzed using the NTP, Pre ranked GSEA and ssGSEA modules from GenePattern (www.genepattern.org) and gene signatures from MSigDB or previously reported (Supplementary Table 1).

Secondly, the in-house validation cohort of 50 HB tumors and 2 adjacent tissues was profiled using the NanoString nCounter Technology with a manually curated list of 65 genes, including HB markers and genes of key signaling pathways (Supplementary Table 2). RNA from tumor FFPE unstained sections was extracted using truXTRAC FFPE RNA microTUBE purification Kits (COVARIS, Woburn, MA). RNA quality control was assessed using Tape Station RNA chips (Agilent) and RNA quality was measured using DV200 metrics. RHOX2 and PNN genes were used as a housekeeping genes. NanoString output files were analyzed by nSolver Analysis Software 4.0.

For the validation cohort, RNA-sequencing data (GSE104766) from tumor and non-tumor HB samples from 25 HB patients were used[23]. Raw expression counts were normalized following the same procedure as previously described[21].

Weighted gene co-expression network analysis

To identify groups of correlated genes that are enriched in tumors compared to non-tumor samples, we used the Weighted gene co-expression network analysis (WGCNA) R package[25]. Networks enriched in tumors were selected based on FDR < 0.001 and module differential connectivity (MDC) ratio < 0.1. Subsequently, to identify the main signaling pathways in each network, we applied the Pathway enrichment module using the Gene Ontology database and selected the top significantly enriched term[26] (all FC > 2 and BH-adjusted p < 0.05). Hub genes (i.e. the top 5 most interconnected genes of the network) were identified based on intra-module connectivity[25]. The selected

genes were filtered for cancer-related genes according to the OncoKB Cancer Gene List (www.oncokb.org) and for targetable alterations using the PANDRUGS database (www.pandrugs.org). Only drugs with high interaction evidence level (i.e. direct targets) were considered.

Classification of *IGF2*^{high} tumor samples

IGF2 overexpression was defined as FC > 4 versus mean tumor adjacent tissue based on qRT-PCR data. For RNA-seq data, a cutoff of FC > 2 versus median tumor adjacent tissue was established based on ROC curve calculations (Supplementary Figure 2, Supplementary Table 3).

Methylation analysis

Methylation data from 27 HB tumors and 22 adjacent non-tumor pairs obtained from a Infinium MethylationEPIC 850K array (Illumina) were previously reported[21] and are accessible through GSE132219. Data were normalized and converted to B values using the ChAMP pipeline[27]. The differential methylation status of the *IGF2* gene promoters in HB tumors and adjacent tissue was conducted using the ChAMP R package (v 2.22.0) by analyzing the array probes located within the maternal allele of adult promoter (P1), fetal promoters (P2, P3 and P4), and ICR1 regulatory region (CTCF-binding site) according to Ensembl Genome Browser (Ensembl.org) and previous studies[18] (Supplementary Table 4). Statistical comparisons for differential methylation analysis were performed using M values[28]. *IGF2* hypomethylation was defined as the mean fold-change of the B-values in the fetal promoter region compared to adjacent non-tumor samples minus standard deviation as previously defined[18].

Loss of heterozygosity analysis

Loss of Heterozygosity (LOH) in HB samples was established from SNP array data of 30 HB tumor samples. SNP array and LOHs data was previously reported[21] and is accessible through GSE132037. Samples with LOH in the chromosomal region 11:2,129,112-2,149,603 from the GRCh38.p12 human genome version were considered positive for LOH in the *IGF2* gene.

219

220 ***Exon-level gene expression and splicing analysis***

221 The *IGF2* exon-level expression analysis was performed using the data of 36 probes of
 222 the Human Transcriptome Array data (GSE132219)[21]. Specifically, expression of
 223 isoforms containing the adult-specific exons 1 (hg19, chr 11: 2,170,833-2,170,356) and
 224 2 (11: 2,169,037-2,168,796) and fetal-specific exon 6 (11: 2,160,619-2,159,459) was
 225 assessed[18]. The supervised differential splicing between tumor and non-tumor
 226 samples as well as IGF2^{high} vs. IGF2^{low} tumors was conducted using Transcriptome
 227 Analysis Console software (ThermoFisher Scientific, Waltham, MA).

228

229 ***Mutational analysis***

230 Mutations were called from paired tumor/normal RNA-Seq data. Mapped RNA-seq
 231 reads were subject to splitting, trimming, local indel realignment, and base-score
 232 recalibration pre-processing with the IndelRealigner and TableRecalibration tools from
 233 Genome Analysis Tool Kit (GATK)[29] under the GATK Best Practices for RNA-seq
 234 paradigm (<https://gatkforums.broadinstitute.org/gatk/discussion/3892/the-gatk-best-practices-forvariant-calling-on-rnaseq-in-full-detail>). MuTect[30] was then used with
 235 default settings to quantify somatic mutation burden. CTNNB1 and AXIN1 alterations
 236 were validated by PCR and Sanger sequencing, as previously described[21].

238

239 ***Identification of TERT promoter mutations:***

240 DNA was extracted from macrodissected fresh frozen (FF) or formalin-fixed paraffin-
 241 embedded (FFPE) tumor tissues using the MagMAX™ DNA Multi-Sample kit (Thermo
 242 Fisher Scientific) or truXTRAC FFPE DNA microTUBE Kit-Column Purification (Covaris).
 243 Qubit was used to quantify DNA concentration and integrity. Then, we performed
 244 polymerase chain reaction (PCR) using specific primers (Forward:
 245 GGTGAAGGGGCAGGACGGGTGC; Reverse: GGCTTCCCACGTGCGCAGCAGGA) and 50 ng
 246 of purified genomic DNA. The PCR reaction was performed by PCR MasterMix (Thermo
 247 Fisher Scientific) including a negative and a positive control. The PCR reaction
 248 conditions were: initial denaturalization 95°C for 2 min, 40 cycles of denaturalization
 249 95°C for 30 sec and annealing 60°C for 30 sec and extension 72°C for 2 min, and a 10
 250 min final extension at 72°C. The PCR product was sequenced by Sanger

Sequencing. Sequencing reactions of both DNA strands were performed with the BigDye® Terminator v3.1 Cycle Sequencing Kit (Thermo Fisher Scientific), run on a Genetic Analyzer ABI 3130 and analyzed with SeqScape v5.3.1 (both from Applied Biosystems). Briefly, 5 µL of PCR product was incubated with 2 µL of illustra ExoProStar 1-Step (GE Healthcare Life Sciences) for 45 min at 37°C and 15 min at 80°C. After purification, 2 µL of purified PCR product was mixed with 2 µL of BigDye Buffer, 1 µL of BigDye, 1.6 µL of 1 µM of primer and 3.4 µL of DNase RNase-free water. The sequencing reaction conditions were: 95°C for 5 min, 96°C for 10 sec, 30 cycles of 50°C for 50 sec, and a 4-min extension at 60°C.

260

261 ***Cell lines and reagents***

HepG2 (ATCC, Manassas, VA) and Huh6 (Japanese Collection of Research Bioresources, Osaka, Japan) HB cell lines were cultured in Dulbecco's Modified Eagle Medium (ThermoFisher, Waltham, MA) supplemented with 10% heat-inactivated fetal bovine serum. Cells were maintained at 37°C in a 5% CO₂ atmosphere. The anti-IGF1/2 monoclonal antibody xentuzumab (BI 836845; see ref. [19] for full sequence and structure) was produced and provided by Boehringer Ingelheim (Ingelheim, Germany) and cisplatin was purchased from Selleckchem (S1166) (Houston, TX). PBS was used as the control.

To generate the 2D PDX-derive cell line, PDX tissue was minced and digested in PBS + 1 mg/mL collagenase IV for 90 minutes at 37°C. Tumor dissociate was strained through a 70 µm strainer and washed with complete RPMI (20% FBS, 1% glutamine, 1% penicillin/streptomycin). 100,000 cells were plated on collagen-coated 35 mm plates in human-2D media (complete RPMI, 40 ng/mL recombinant human EGF, 10 uM Y-27632, and 5 uM A83-01). Cells were cultured and maintained in human-2D media 37°C in a 5% CO₂ atmosphere.

277

278 ***In vitro functional cell assays***

Cell proliferation and colony formation capacity were evaluated in HepG2 (ATCC, Manassas, VA), Huh6 (Japanese Collection of Research Bioresources, Osaka, Japan) and 2D PDX-derived cells treated with xentuzumab (Boehringer Ingelheim, Ingelheim, Germany), cisplatin (Selleckchem, Houston, TX), its combination, or vehicle. For the

matrix viability assay, 4000 cells/well were seeded in 96-well plates for 24h in a humidified atmosphere at 37°C and 5% CO₂. Thereafter, cells were incubated for 72h with increasing concentrations of cisplatin and xentuzumab. Cell viability was measured with absorbance at 560 and 590 nm from resazurin. Combination index values were calculated for each column and averaged across each matrix. To assess colony formation capacity, 600 cells/well were seeded in 6-well plates. After 24h, Huh6 and HepG2 cells were treated with cisplatin (0.3 μM), xentuzumab (1 μM) or their combination and incubated for 12 days, with drug-containing media changed three times per week. Thereafter, cells were rinsed with cold PBS, fixed with methanol and stained with 0.5% Crystal Violet (Sigma-Aldrich, Saint Louis, MO). The number of colonies was manually counted. All experiments were performed in triplicate.

Establishment of the PDX-derived organoid model

A patient-derived HB tumor with high *IGF2* expression provided by Xentech (Evry, France)[31] was implanted and grown subcutaneously in 6-8 week-old female NOD/SCID immunosuppressed mice (n = 3; Charles River Laboratories, Wilmington, MA). Animals were weighed and tumor volume was assessed three times per week using bilateral caliper measurements according to the formula $volume = length \times width^2 \times 0.5$. Once tumors reached 1000 mm³, the animals were sacrificed and tumors were collected to generate three independent organoid lines (PDX-derived organoids). Histological and molecular characterization of the PDX have been reported elsewhere (PDX ID: HB-235)[31]. To generate the organoids[32], PDX tumors were minced and digested in sterile digestion media (PBS, 0.125 mg/mL collagenase from clostridium histolyticum, 0.125 mg/mL dispase II, and 0.1 mg/mL DNaseI) for two hours at 37°C. Tumor dissociates were strained through a 70 μm strainer and washed with basal media (Advanced DMEM/F-12, 1% glutamine, 1% penicillin/streptomycin, 10 mM HEPES). Cell dissociates were cultured at 50,000 cells per 50 μL Matrigel (Corning) in 24 well plates in human tumor organoid media (basal media, 1:50 B27 no vitamin A, 1:100 N2, 1 mM N-acetylcysteine, 10% Rspo1-conditioned media, 10 mM nicotinamide, 10 nM recombinant human [Leu¹⁵]-gastrin I, 50 ng/mL recombinant human EGF, 100 ng/mL recombinant human FGF10, 25 ng/mL recombinant human HGF, 10 μM forskolin, and 5 μM A83-01). Studies were performed in compliance with the “Guide

for the Care and Use of Laboratory Animals” and they were approved by the Institutional Animal Care and Use Committee (IACUC-2016-0296).

317

318 ***Antitumor effect of IGF2 inhibition in an IGF2^{high} organoid model***

Organoids were seeded and treated with serial dilutions of cisplatin (Selleckchem, Houston, TX) or xentuzumab (Boehringer Ingelheim, Ingelheim, Germany) for cell viability analyses and IC₅₀ calculations. After 3 days of incubation, cell viability was measured with absorbance at 560 and 590 nm from resazurin. Combination index values were calculated for each column and averaged across each matrix.

Caspase-dependent apoptosis was assessed by measuring caspase-3 and -7 activity (Caspase-Glo 3/7 Assay, Promega). Organoids were treated with or without 100 nM of IGF2 (Preprotech, Rocky Hill, NJ) and increasing concentrations of xentuzumab (0, 1, 10, 100 μM) and cisplatin (0, 1, 5 μM). All organoid experiments were performed using the 3 independent organoid lines and in technical triplicates.

329

330 ***IGF2^{high} xenograft murine model***

To generate the xenograft murine model of IGF2^{high} HB, 5x10⁶ HepG2 cells were subcutaneously injected into the right flank of immunocompromised 6-8 weeks-old athymic (nu/nu) (Crl:NU-Foxn1nu) female mice (n = 55 mice; Charles River Laboratories, Wilmington, MA). Animals were weighed and tumor volume was assessed 3 times per week using bilateral caliper measurements according to the following formula: $volume = length \times width^2 \times 0.5$. When tumors reached 150 mm³, animals were randomly assigned to receive xentuzumab (n = 14), cisplatin (n = 13), combination therapy (xentuzumab plus cisplatin, n = 14) or drug vehicle (n = 14). Xentuzumab (100 mg/kg) was administered twice per week; and cisplatin (2 mg/kg) was administered daily. Both drugs were administered intraperitoneally. Body weight, tumor growth and survival (defined as time to reach 1500 mm³) were monitored in all the mice. Once animals reached the survival endpoint, they were sacrificed following Institutional Animal Care and Use Committee guidelines. Studies were performed in compliance with the “Guide for the Care and Use of Laboratory Animals” and they were approved by the Institutional Animal Care and Use Committee (IACUC-2016-0296).

347

348 ***IHC analysis***

349 Tumor samples from the mouse model were fixed in buffered 4% paraformaldehyde
 350 for 24 hours and embedded in paraffin to create formalin-fixed paraffin-embedded
 351 (FFPE) blocks. An expert pathologist blinded to the treatment arms (CM) assessed the
 352 percentage of viable and necroapoptotic tissue in H&E-stained slides. This was used
 353 together with the ex-vivo tumor volume to calculate the viable and necroapoptotic
 354 tumor volume. CD31 staining (Abcam ab28364) was assessed by IHC on 3 μ m-thick
 355 FFPE tissue sections after heat-induced antigen retrieval and quantified by the digital
 356 pathology imaging software QuPath (version 0.2.0). To ensure representative sampling
 357 of the entire tumor, 5 regions of interest were analyzed.

358

359 ***Western blotting***

360 Huh6 and HepG2 cells and organoids were stimulated with 100 nM of IGF2
 361 (PeproTech, East Windsor, NJ) to induce IGF1R pathway activation, along with cisplatin
 362 (0.3 μ M for cell lines and 1 μ M for organoids), xentuzumab (0.1 μ M), its combination
 363 or vehicle. For Huh6 and HepG2 cell lines, after 24h of stimulation, cells were washed
 364 with PBS, collected by scraping and lysed in lysis buffer (50 mM Tris pH=7.4, 150 mM
 365 NaCl, 1% Triton X-100, 0.1% SDS, 0.25 mM EDTA, 1% Sodium deoxycholate) containing
 366 protease and phosphatase inhibitors. For organoids, after 24h of stimulation,
 367 organoids were collected in Cell Recovery Solution (Corning, Corning, NY), and matrigel
 368 was dissolved by rotation for 1h at 4°C. Pelleted organoids were then lysed in 2X
 369 Laemmli sample buffer containing 4% of 2-mercaptoethanol, heated at 95°C for 10min,
 370 sonicated, and heated again at 95°C for 5min. Protein concentration was determined
 371 using Protein Assay Dye Reagent Concentrate (Bio-Rad, Hercules, CA) and bovine
 372 serum albumin (BSA) was used as a standard. Protein extracts were resolved by SDS-
 373 PAGE and transferred onto polyvinylidene difluoride membranes by western blot.
 374 Membranes were blocked with 3% BSA and incubated overnight at 4°C with primary
 375 antibodies. Horseradish peroxidase-conjugated secondary antibodies were applied at
 376 room temperature for 1h. The specifications and dilutions of antibodies used for
 377 Western Blotting are listed in Supplementary Table 5. Blots were developed using ECL

plus solution (GE Healthcare, Waukesha, IL) and imaged with the FUJI film Laser Image Analyzer.

Quantitative real-time PCR

The expression of IGF2 from promoter 1 (adult isoform), promoter 3 (fetal isoform), total IGF2, IGF1R, H19, and TGF- β mRNA levels were tested in the following sets of samples: HB tumor samples (n = 27), paired adjacent non-tumor liver samples (n = 25), HB cell lines (HepG2 and Huh6 cells), organoids and, as controls, healthy liver samples (n = 5, from patients with focal nodular hyperplasia or cystadenoma, without underlying liver disease). Total RNA from tissues and cell lines was isolated using the RNeasy Mini Kit (Qiagen, Hilden, Germany). The cDNA was reverse transcribed from 1 μ g of total RNA using RNA to cDNA EcoDry Premix Double Primed (Clontech, Takara Biotechnology, Dalian, China) in a total volume of 20 μ l. Quantitative real time PCR was performed using TaqMan probes for *IGF2*-P1 (Hs01005962-m1), *IGF2*-P3 (Hs00171254-m1), *IGF2*-P1/2/3 (Hs01005963-m1), *IGF1R* (Hs00609573-m1), *H19* (Hs00262142_g1), and *TGF- β* (Hs00998133-m1). Each sample was analyzed in triplicate and normalized to the internal control 18S ribosomal RNA (Hs99999901-s1). The fold change of mRNA expression in tumor tissue was calculated referring to the average mRNA expression levels in adjacent non-tumor tissue.

To assess miR-483-5p expression levels, microRNA from tumor and paired adjacent tissue was obtained using the TaqMan MicroRNA Reverse Transcription Kit (ThermoFisher Scientific), and qRT-PCR was performed following the TaqMan Small RNA assay and TaqMan probes for miR-483-5p (ThermoFisher Scientific, 002338). Each sample was analyzed in triplicate and normalized to the internal control miR-361-5p (ThermoFisher Scientific, 000554). Fold change was calculated referring to the averaged mRNA expression levels in adjacent non-tumor tissue.

Statistical analysis

Statistical analyses were conducted using R (version 3.6.2, R Foundation for Statistical Computing, Vienna, Austria). Comparisons of continuous variables were performed using Kruskal-Wallis and Dunn's tests for non-parametric distributions, or ANOVA and Tukey tests for parametric distributions. Correlations for categorical variables were

analyzed using Fisher's exact test. Survival and time to response were assessed with Kaplan-Meier estimates and log-rank test.

Data availability

The data generated in this study including RNA-sequencing, methylation and SNP array are available within the article, its supplementary data files, and in Gene Expression Omnibus (GSE104766, GSE132219 and GSE132037). Data from validation cohorts were obtained from Gene Expression Omnibus (GSE132219 and GSE104766).

RESULTS

IGF signaling is highly deregulated in HB

To identify molecular alterations driving oncogenesis in HB, we used RNA-seq data from a cohort of 31 HB tumors[21] (29 HBs and 2 HCN-NOS) and matched non-tumor tissues (study cohort, Supplementary Figure 1, Table 1). Through gene co-expression network analysis, we identified seven network modules that were significantly differentially expressed between tumor and non-tumor samples from the study cohort. The top enriched gene ontology terms in these network modules included IGF2 signaling pathway (module 1), cell cycle and survival (modules 6-7), and immune response (modules 2-3) (FDR<0.001, Supplementary Table 6). Notably, the Wnt signaling pathway, which is a commonly deregulated in HB[21], was also enriched in the network module 1 (GO:0016055, $p = 0.009$). We also explored the top interconnected genes within each network (hub genes) and identified several targetable cancer-related candidates including IGF2, TGFB1, and BIRC3 (Supplementary Figure 3). Notably, *IGF2* was the targetable gene with the highest expression levels in the study cohort (Supplementary Figure 3, Supplementary Tables 7-8), making it the most suitable candidate for our study.

We then assessed the rate of HB tumors overexpressing *IGF2* in the study cohort. Of the 31 HBs, 22 (71%) were classified as *IGF2*^{high} based on RNA-seq data ($FC > 2$ vs non-tumor adjacent tissue), and this was aligned with the *IGF2* levels measured by qRT-PCR (Figure 1A and 1B) and with previous studies[14, 15]. Additionally, *IGF2* pathway deregulation was also observed at the level of *IGF1R* and *H19* (Supplementary Figure 4), in line with other reports[33].

These results were confirmed in two independent cohorts: in the first, our in-house validation cohort (n=50), 78% of patients (39/50) exhibited high levels of IGF2; and in the second[23], 76% (19/25) (Supplementary Figure 4).

Overall, our results indicate that *IGF2* overexpression is the main targetable alteration among the top deregulated pathways in our HB cohort, and is present in 70-80% of cases.

IGF2^{high} HB tumors are enriched in high risk HB molecular classes

We analyzed the transcriptomic and methylation profile of the study cohort to gain further insight into the molecular characteristics of IGF2^{high} HB tumors (Figure 1B, Supplementary Figure 5). IGF2^{high} tumors were enriched in high-risk molecular classes of HB including the MRS-3, the C2-pure, the C2A and the “Liver progenitor” classes of HB[15, 21, 23, 34]), as well as the EpiCB epigenetic cluster signature[21], and the HCC proliferation class[35]. IGF2^{high} tumors also showed enrichment in progenitor cell markers (*EPCAM*, *AFP*, *DLK1* and *PEG3*) and gene sets associated with cell cycle progression (Figure 1B, Supplementary Figure 5). Only 1 out of 31 cases were found to have *TERT* promoter mutations, and this single case corresponded to an HCN-NOS tumor. In terms of clinical features, IGF2^{high} patients presented shorter recurrence-free survival after resection than IGF2^{low} patients (median 34 months vs not reached for IGF2^{low}; p = 0.02, Figure 1C), which align with their molecular features. No additional clinicopathological differences were observed between IGF2^{high} and IGF2^{low} tumors (Table 1).

In contrast, tumors with low IGF2 levels (IGF2^{low}; 9/31, 29%) were enriched in low-risk and mesenchymal HB classes (MRS-1, C2B and “Mesenchymal” HB classes[15, 21, 23]), together with gene sets associated with inflammatory and interferon signaling, TGF-β pathway activation and epithelial-to-mesenchymal transition (Figure 1C). The high presence of inflammatory signaling was confirmed with gene signatures capturing specific immune cell populations including cytotoxic T cells (Supplementary Figure 5). The expression levels of *TGFB1* and TGF-β pathway-related genes were higher in IGF2^{low} tumors than in IGF2^{high} and non-tumor samples (all p < 0.0001, Supplementary Figure 5). These results indicate that IGF2^{low} tumors present a mesenchymal and highly

infiltrated phenotype, which is in line with their association with a better outcome compared to IGF2^{high} tumors.

These molecular features of IGF2^{high} and IGF2^{low} HBs were confirmed in an independent HB cohort of 25 patients[23]. In line with our data, gene expression analysis in the external cohort revealed enrichment of proliferation and cell cycle-related gene sets in IGF2^{high} tumors, compared to inflammatory and interferon signaling in IGF2^{low} cases (FDR < 0.05, Supplementary Figure 5).

480

481 ***Fetal promoter hypomethylation, ICR1 deregulation, LOH and miR-483-5p levels drive*** 482 ***IGF2 overexpression in HB***

Next, we investigated the mechanisms of *IGF2* overexpression in HB. Previous reports have described aberrant IGF2 levels in HB associated with hypomethylation of the fetal P2, P3, and P4 promoters, as opposed to physiological P1-mediated expression[36]. Here, we used methylation 850K-array data to assess the methylation differences between IGF2^{high} and IGF2^{low} tumors. Tumors with high *IGF2* expression levels presented significantly decreased methylation of the *IGF2* fetal promoters compared to tumors with low *IGF2* levels (Figure 2A, Supplementary Figure 6). In particular, *IGF2* fetal promoter hypomethylation was present in 50% of IGF2^{high} samples (9/18 vs 1/9 in IGF2^{low} samples, $p < 0.05$; Figure 3). To assess whether the hypomethylation of the *IGF2* fetal promoter correlated with higher expression of its fetal isoform, we expanded our analysis to the *IGF2* splicing profile based on an HTA (Human Transcriptome Array) expression array at exon level. Our data demonstrated that the *IGF2* fetal isoform was overexpressed in IGF2^{high} tumors compared to IGF2^{low} tumors (Figure 2B-C). Furthermore, overexpression of the fetal *IGF2* isoform in IGF2^{high} was confirmed by qRT-PCR in both the study cohort and in-house validation cohort (Supplementary Figure 6). Our results suggest that IGF2^{high} HB tumors present a fetal *IGF2* expression pattern through hypomethylation of the fetal promoters. In addition, we also identified gain of methylation in the *IGF2/H19* imprinting region ICR1 of IGF2^{high} tumors, in line with previous studies[15]. Particularly, ICR1 gain of methylation was present in 61% of IGF2^{high} patients (11/18 vs 1/9 in IGF2^{low} samples, $p < 0.05$; Figure 3, Supplementary Figure 6).

504 Additionally, the 11p15.5 imprinted locus, which contains *IGF2*, has also recently been
 505 reported as the second most frequently altered locus in hepatoblastoma[15], mostly
 506 through copy-neutral loss of heterozygosity (LOH). Since *IGF2* presents monoallelic
 507 expression in normal conditions, LOH in this genomic region increases its
 508 expression[14, 37]. We used our SNP array data to determine the rates of this allelic
 509 imbalance in $IGF2^{high}$ vs $IGF2^{low}$ HB tumors. $IGF2^{high}$ tumors were significantly enriched
 510 in 11p15.5 LOH compared to $IGF2^{low}$ tumors [12/21 (57%) vs 1/9 (11%), $p < 0.05$, Figure
 511 2D-E, Figure 3]. Interestingly, the four $IGF2^{high}$ HB samples corresponding to infant
 512 patients (< 8 months of age) showed 11p15.5 LOH (Figure 3), which suggests that their
 513 *IGF2* overexpression was not due to physiological regulation in fetal and early
 514 postnatal stages[38], but due to genetic aberrations.

515 Finally, the expression of the micro-RNA miR-483-5p has been reported to promote
 516 fetal *IGF2* transcription by binding to its 5' untranslated region (UTR)[39] and as a
 517 mechanism of *IGF2* overexpression in HCC[18]. In our study cohort, miR-483-5p levels
 518 were significantly higher in $IGF2^{high}$ HB tumors than in $IGF2^{low}$ HB tumors, both
 519 according to the FC vs adjacent non-tumor tissue in RNA-seq (2.4 vs 0.7, $p < 0.05$) and
 520 qRT-PCR data (3.2 vs 0.6, $p < 0.001$) (Figure 2F). Overall, miR-483-5p overexpression,
 521 defined as FC > 2 vs adjacent non-tumor samples, was detected in 55% (11/20) of
 522 $IGF2^{high}$ HB tumors and only in 11% of $IGF2^{low}$ tumors ($p < 0.05$; Figure 3).

523 Altogether, our results indicate that *IGF2* overexpression in HB is driven by
 524 hypomethylation of its fetal promoters, ICR1 deregulation, LOH in 11p15.5, and miR-
 525 483-5p expression. Most $IGF2^{high}$ HB patients [91% (20/22)] presented at least one of
 526 these mechanisms of *IGF2* overexpression (Figure 3).

527

528 ***IGF2^{high} HB cells present high sensitivity to IGF2-inhibition***

529 The presence of *IGF2* overexpression in 71% of HB patients and their poor outcome
 530 prompted us to test IGF2 blockage in HB. In addition, the monoclonal antibody against
 531 IGF1 and IGF2, named xentuzumab, has shown promising antitumor effects in other
 532 cancer types[20]. To this end, the antitumor effects of xentuzumab were evaluated *in*
 533 *vitro* (HB cell lines and HB PDX-organoids) and in an *in vivo* murine model of HB. The
 534 effects were compared to those of a conventional therapeutic agent for HB patients
 535 (cisplatin)[5]. *IGF2* expression levels in HB cell lines (HepG2 and Huh6) were assessed

by qRT-PCR (Supplementary Figure 7). HepG2 cells presented high *IGF2* expression, defined as FC > 4 compared to non-tumor adjacent tissue (median FC = 19.60), and were used as a model to recapitulate *IGF2*^{high} HB tumors. Conversely, Huh6 cells showed low *IGF2* expression (median FC = 0.04; Supplementary Figure 7) and thus were considered to phenocopy the *IGF2*^{low} HBs. As observed in *IGF2*^{high} human HB tumors, HepG2 cells also showed high expression of the receptor *IGF1R*, low *H19* expression, and high expression of the fetal isoform of *IGF2* (P2-4 derived) (Supplementary Figure 7). Previous studies[14] have reported that HepG2 cells present fetal promoter hypomethylation and LOH genomic imbalances as opposed to Huh6. For validation purposes, we generated a cell line derived from a human PDX model with high expression of *IGF2* (hereinafter referred to as PDX-derived cell line). We tested the effect of *IGF2* blockade and chemotherapy in *IGF2*^{high} cells (HepG2 and PDX-derived cell line) and *IGF2*^{low} cells (Huh6). In *IGF2*^{high} cells, xentuzumab strongly decreased cell viability in combination with low doses of cisplatin (0.1 – 1 μ M), where cisplatin was not effective as monotherapy, eliciting a strong synergistic effect (Combination Indexes: HepG2, CI = 0.47; PDX-derived cells, CI = 0.44; Figure 4A, Supplementary Figure 7). In contrast, the synergism of *IGF2* blockade and chemotherapy was not observed in Huh6 cells (*IGF2*^{low}), where the anti-proliferative effects were mainly driven by cisplatin, with a mild added effect of xentuzumab (CI = 0.94, Figure 4A). Consistently, xentuzumab in combination with cisplatin reduced the colony formation capacity of *IGF2*^{high} HepG2 cells compared to monotherapies, including cisplatin (all $p < 0.05$, Figure 4B). Conversely, the combination treatment did not show significant differences in the Huh6 cell line compared to monotherapies. When comparing the effect of the combination, this was 5.1-fold stronger in HepG2 cells (*IGF2*^{high}) than in Huh6 cells (*IGF2*^{low}), corresponding to a 46% vs 9% reduction, respectively ($p < 0.001$, Supplementary Figure 7). On the other hand, xentuzumab alone induced significant differences in colony formation compared to the control (all $p < 0.01$), but it did not induce superior antitumor effects compared to cisplatin monotherapy (Figure 4B). The impact of xentuzumab alone in HepG2 cells was between 4.5-fold stronger than in Huh6 cells (22% vs 5%, $p < 0.01$; Figure 4B and Supplementary Figure 7).

Overall, the IGF1/2 inhibitor xentuzumab in combination with cisplatin strongly reduced the proliferation and colony formation capacity of HB cells, and this effect was more pronounced in *IGF2^{high}* cells than in *IGF2^{low}* cells.

The combination of IGF2 inhibition and cisplatin elicits synergistic effects in IGF2^{high} HB organoids

Considering the antitumor capacity of IGF2 inhibition with xentuzumab combined with cisplatin observed in *IGF2^{high}* HB cell lines, we proceeded to further evaluate the antitumor and molecular effects of this combination in more complex experimental models such as organoids derived from a PDX murine model generated from an *IGF2^{high}* HB tumor[31]. First, we confirmed by RT-PCR that the high *IGF2* levels in the original HB tumor were maintained in the organoids. Indeed, *IGF2* levels in the organoid model were 19.5-fold higher when compared to mean *IGF2* levels of the adjacent human liver tissue (Supplementary Table 9).

Next, organoids were treated with xentuzumab, cisplatin, xentuzumab + cisplatin, or control IgG, and organoid viability was assessed. A strong synergistic reduction in cell viability was observed with the combination of low doses of xentuzumab (1 nM) and cisplatin (< 1 μ M), where monotherapies were not effective (combination index: 0.43; Figure 4C). A synergistic peak was observed for 1 μ M cisplatin and 100 nM xentuzumab. This was further confirmed by calculating the IC₅₀ for each condition. Indeed, the IC₅₀ obtained for cisplatin combined with 0.1 μ M xentuzumab was 25-fold lower than the one obtained for cisplatin as monotherapy (99.19 nM vs 2.57 μ M), while the IC₅₀ for xentuzumab alone was not reached with the assessed concentrations (>100 nM) (Figure 4D, Supplementary Figure 8).

Next, we investigated the effect of the combination of xentuzumab and cisplatin at low concentrations. The combination of xentuzumab and cisplatin activated apoptosis in a dose-dependent manner in organoids (Figure 4E), while monotherapies did not. The combination also reduced the activation of the IGF1R pathway, as measured by western blotting of IGF1R and Akt phosphorylation, in both organoids and cell lines stimulated with IGF2 (Figure 4F, Supplementary Figure 9). Intriguingly, xentuzumab reduced IGF2 pathway activation, but this effect was markedly enhanced by the

598 combination, partially explaining the synergism of the combination and stressing the
599 importance of combining both treatments to obtain antitumoral responses.

600 Therefore, these data validate the results observed in cell lines, suggesting that the
601 efficacy of cisplatin could be greatly improved by the combination with IGF2 inhibition
602 in IGF2^{high} HB patients.

603

604 ***The combination of IGF2 inhibition and cisplatin is more effective than cisplatin alone***
605 ***in a murine model of IGF2^{high} HB***

606 The antitumor potential of IGF2 inhibition in combination with chemotherapy was
607 tested in a xenograft murine model of IGF2^{high} HB, generated through subcutaneous
608 implantation of HepG2 cells. Mice bearing HB tumors were randomized to receive
609 cisplatin, xentuzumab, cisplatin + xentuzumab, or control IgG. Mice treated with the
610 combination of xentuzumab and cisplatin showed significantly increased survival
611 (median survival: 16 days) compared to those treated with cisplatin alone (10 days, $p =$
612 0.038 vs combination) or IgG control (13 days, $p = 0.027$ vs combination) (Figure 5A).
613 Conversely, the monotherapy treatment arms were unable to significantly reduce the
614 viable tumor volume compared to the control. No significant differences in body
615 weight or other toxicity signs were observed, indicating that all treatments were well-
616 tolerated (Supplementary Figure 10).

617 Next, we analyzed the tumors and the antitumor effects of the treatments at the
618 histological level. The combination of cisplatin and xentuzumab significantly decreased
619 the fraction of viable tumor volume compared to cisplatin alone ($p < 0.01$) and the
620 control ($p < 0.05$; Figure 5B-C). Furthermore, CD31 expression, a well-defined marker
621 of angiogenesis, was significantly decreased in tumors from the combination
622 treatment and cisplatin alone, likely because of the previously reported anti-
623 angiogenic effect of cisplatin treatment and IGF1/2 blockade[18, 40] (Figure 5D).

624 Overall, these results indicate that the combination of xentuzumab and cisplatin
625 improved survival and showed an increased antitumor effect compared to cisplatin
626 alone. In addition, our data provide the rationale for testing IGF2 inhibitors in
627 combination with cisplatin in trials with HB patients that express high levels of IGF2.

628

629 DISCUSSION

630 HB is a rare pediatric liver cancer that has largely been understudied at the molecular
 631 level. Recently, the molecular profile of these tumors has been deciphered using multi-
 632 omics approaches[9, 15, 21, 23, 41]. Despite these efforts, there are still no available
 633 targeted therapies in HB. Hence, HB patients receive standard preoperative platin-
 634 based chemotherapy regimens[3], associated with serious adverse effects, which could
 635 be partially avoided with other therapeutic approaches[7]. Herein, we provide
 636 evidence suggesting that *IGF2* overexpression is a targetable alteration in HB
 637 (considering HBs and HCN-NOS), and describe the epigenetic mechanisms of *IGF2*
 638 overexpression. Additionally, we showed remarkable antitumor effects of the
 639 combination of IGF2 inhibition and cisplatin in preclinical models.

640 Gene co-expression network analysis revealed that IGF2/IGF1R signaling is one of the
 641 most deregulated pathways in HB. In line with previous studies showing high IGF2
 642 levels in HB[14, 42], *IGF2* overexpression was detected in 71% of HB cases, being the
 643 most overexpressed targetable gene in tumors compared to non-tumor tissue. *IGF2*
 644 overexpression is associated with progenitor cell markers (*EPCAM*, *AFP*, *DLK1* and
 645 *PEG3*) and HB molecular classes of high-risk tumors (C2[21, 34], MRS-3[21]). In line
 646 with this, it has been reported that genes with epigenetic regulation such as *IGF2* are
 647 abundantly expressed in the fetal liver[43] and that HB tumors with liver progenitor
 648 features are highly proliferative and have poor survival[15, 34]. On the other hand,
 649 *IGF2*^{low} tumors were associated with a mesenchymal HB phenotype, with higher
 650 presence of EMT and TGF- β signaling markers, together with higher immune infiltrate.
 651 Importantly, patients with *IGF2*^{high} tumors presented poorer recurrence-free survival
 652 compared to *IGF2*^{low} tumors, highlighting the need for new therapies for this subgroup
 653 of patients[44].

654 *IGF2* is a well-known paternally imprinted gene that encodes a fetal peptide hormone
 655 that regulates cellular proliferation and differentiation during the early stages of
 656 development[45]. It is highly expressed in the liver during fetal stages from the
 657 promoters P2, P3, and P4, and in adulthood, it is expressed from both alleles of
 658 promoter P1, albeit at much lower levels[36]. Reactivation of *IGF2* expression through
 659 fetal promoter demethylation has been described as a crucial mechanism for *IGF2*
 660 overexpression in liver cancer[18, 41, 46]. Other mechanisms of *IGF2* overexpression in

cancer involve ICR1 deregulation[15, 47], LOH of the 11p15.5 region[14, 15] and miR-483-5p expression[18, 48]. Our integrative analysis revealed that these four mechanisms are pivotal in driving *IGF2* overexpression in HB, explaining 91% of the cases of *IGF2*^{high} HB. Others have previously suggested a complex interaction between IGF and Wnt/ β -catenin signaling and potential activation of IGF1R signaling due to *CTNNB1* mutations in colon cancer[49, 50].

The high prevalence of *IGF2* overexpression in HB and its association with poor outcomes make it an excellent candidate as a targetable alteration to develop personalized therapeutic approaches, since targeted therapeutic options for these patients are urgently needed. Targeted inhibition of IGF1/2 ligands with xentuzumab abrogates proliferative signaling through IGF1R, without affecting metabolic cell functions[18, 51]. Earlier studies in HCC pointed to the receptor IGF1R as a potential target[17]; however, subsequent clinical trials blocking this receptor using IGF1R mAb or IGF1R/insulin receptor (INSR) tyrosine kinase inhibitors failed to demonstrate beneficial outcomes[44] and resulted in metabolic-related toxic effects due to the inhibition of insulin metabolic signaling. Therefore, xentuzumab has important advantages over previous attempts to inhibit the IGF2/IGF1R pathway.

In HCC and colon cancer *in vivo* models, xentuzumab has shown encouraging antitumor activity and a favorable safety profile, specific for *IGF2*^{high} tumors[18, 51]. A potent antiproliferative effect of xentuzumab has also been reported in cell lines from several cancer types, including HCC and HB[15, 18]. This promising background prompted us to further evaluate the potential of xentuzumab as a new targeted therapy for *IGF2*^{high} HB tumors by assessing its effects on tumor organoids and a murine xenograft model. In this regard, xentuzumab combined with cisplatin significantly improved the effects of the compounds administered as monotherapy. Specifically, xentuzumab in combination with cisplatin was able to improve by 25-fold the efficacy of cisplatin alone in HB organoids and demonstrated an enhanced antitumor effect in *IGF2*^{high} cells compared to *IGF2*^{low}, indicating a new treatment strategy that would increase survival in *IGF2*^{high} HB patients. In addition, the combination was effective at low cisplatin doses, suggesting that - in this setting - chemotherapy doses could be reduced and the chemotherapy-related adverse events diminished. This is especially important considering that chemotherapy causes serious

adverse effects in HB patients such as ototoxicity[7, 52], which is detrimental to language and social development, particularly in young children[53]. Of note, patient stratification based on IGF2 tumor levels at time of diagnosis would be required in clinical studies testing xentuzumab in HB.

On the other hand, in other tumor types, treatment with IGF2/IGF1R inhibitors has been demonstrated to reactivate the antitumor effect of DNA-damaging agents such as cisplatin[54]. Our results support the idea that IGF1R pathway inhibition enhances sensitivity to DNA-damaging agents, as we see reactivation of the efficacy of cisplatin in the combination setting both in our HepG2 xenograft model and in our *in vitro* models.

The combination reduced aberrant angiogenesis, as observed by CD31 staining, similarly than monotherapies, and in line with the previously described anti-angiogenic effects of xentuzumab and cisplatin[18, 40] in other tumor types. Specifically, both IGF2 blockage and cisplatin have been reported to inhibit aberrant vasculature formation by downregulating VEGF signaling[55] and promoting the release of matrix metalloproteinases[40], respectively.

One limitation of the current study lies in the lack of specific cellular models for each of the newly described HB subtypes. Thus, despite HepG2 cells lines have been recently suggested to be derived from an HCN-NOS hepatoblastoma tumors[10], in the present study were used as model overall representing HB cases with high levels of IGF2. In this sense, clinical studies are awaited to clarify whether patients with HCN-NOS tumors need to be managed different from patients with HB tumors.

A second limitation of the study was the use of post-chemotherapy specimens. Here, we acknowledge that the implementation of our findings into the clinical setting will require further validation in diagnostic biopsies and the evaluation of the safety and antitumoral effects of the combination in ad-hoc pre-clinical models.

Overall, this study defines *IGF2* as a promising molecular target in HB and provides evidence that IGF2 inhibition with xentuzumab enhances the efficacy of cisplatin. Therefore, combining xentuzumab with cisplatin could exert a greater antitumor effect than cisplatin alone in a subset of HB patients (~70%) presenting *IGF2* overexpression. This provides a preclinical rationale for exploring this targeted therapy in combination with cisplatin in patients with IGF2^{high} HB.

725

726 **ACKNOWLEDGEMENTS**

727 We thank Dr. Catherine Guettier, from the Université Paris-Saclay, for the pathological
728 review of the samples included in the study.

729 This study was funded by a grant from Boehringer Ingelheim. **J. Abril-Fornaguera** was
730 supported by the PREDOCS-UB grant from the University of Barcelona (UB) and by a
731 mobility grant from Fundació Universitària Agustí Pedro i Pons. **J. Carrillo-Reixach** and
732 **A. Del Río-Álvarez** were supported by the Catalan Agency for the Management of
733 University and Research Grants (AGAUR, 2019 FI_B01024 and 2022_FI_B00528). **U.**
734 **Balaseviciute** was supported by the EILF-EASL Juan Rodés PhD Studentship from the
735 European Association for the Study of the Liver (EASL) and the EASL International Liver
736 Foundation (EILF). **R. Pinyol** was supported by the University of Barcelona (UB) and
737 IDIBAPS/Fundació Clínic Barcelona. **C. Montironi** was supported by a Rio Hortega grant
738 from Instituto de Salud Carlos III (ISCIII), Fondo Social Europeo (CM19/00039). **P. K.**
739 **Haber** was supported by the fellowship grant of the German Research Foundation
740 (DFG/HA 8754/1-1). **M. Puigvehí** received a Juan Rodés scholarship grant from
741 Asociación Española para el Estudio del Hígado (AEEH). **C. E. Willoughby** was
742 supported by a Sara Borrell fellowship (CD19/00109) from the ISCIII and Fondo Social
743 Europeo. **J. Peix** received support from the Generalitat de Catalunya (PERIS,
744 SLT017/20/000206). **E. Guccione** was supported by Alex's Lemonade Stand
745 Foundation. **D. Sia** was supported by the Gilead Sciences Research Scholar Program in
746 Liver Disease. **C. Armengol** received funding from Instituto de Salud Carlos III
747 (PI10/02082, PI13/02340), the European Union's Horizon 2020 research and
748 innovation program under grant agreement N° 668596 (ChiLTERN) and N° 826121
749 (iPC), CIBERehd (CB06/04/0033), AGAUR (2017-SGR-490) and the Ramón y Cajal (RYC-
750 2010-07249) program of the Spanish Ministry of Science and Innovation. **J. M. Llovet**
751 was supported by grants from the Samuel Waxman Cancer Research Foundation; the
752 Spanish National Health Institute (MICINN, PID2019-105378RB-I00); NIH (R01
753 DK128289-01); through a partnership between Cancer Research UK (CRUK),
754 Fondazione AIRC per la Ricerca sul Cancro and Fundación Científica de la Asociación
755 Española Contra el Cáncer (FAECC) (Accelerator Award, HUNTER, Ref. C9380/A26813);
756 and by grants from the Acadèmia de Ciències Mèdiques i de la Salut de Catalunya i

757 Balears; and the Fundación Científica de la Asociación Española Contra el Cáncer
758 (FAECC; Ref. PRYGN223117LLOV).

759

760 REFERENCES

- 761 [1] Schnater JM, Köhler SE, Lamers WH, et al. Where do we stand with hepatoblastoma?
762 *Cancer* 2003; 98: 668–678.
- 763 [2] Linabery AM, Ross JA. Trends in childhood cancer incidence in the U.S. (1992–2004).
764 *Cancer* 2008; 112: 416–432.
- 765 [3] Feng J, Polychronidis G, Heger U, et al. Incidence trends and survival prediction of
766 hepatoblastoma in children: a population-based study. *Cancer Commun* 2019; 39: 62.
- 767 [4] Nussbaumer G, Benesch M. Hepatoblastoma in molecularly defined, congenital
768 diseases. *Am J Med Genet A* 2022; 188: 2527–2535.
- 769 [5] Kremer N, Walther AE, Tiao GM. Management of hepatoblastoma. *Curr Opin Pediatr*
770 2014; 26: 362–369.
- 771 [6] Semeraro M, Branchereau S, Maibach R, et al. Relapses in hepatoblastoma patients:
772 Clinical characteristics and outcome – Experience of the International Childhood Liver
773 Tumour Strategy Group (SIOPEL). *Eur J Cancer* 2013; 49: 915–922.
- 774 [7] Knight KR, Chen L, Freyer D, et al. Group-Wide, Prospective Study of Ototoxicity
775 Assessment in Children Receiving Cisplatin Chemotherapy (ACCL05C1): A Report From
776 the Children’s Oncology Group. *J Clin Oncol* 2017; 35: 440–445.
- 777 [8] López-Terrada D, Alaggio R, De Dávila MT, et al. Towards an international pediatric liver
778 tumor consensus classification: proceedings of the Los Angeles COG liver tumors
779 symposium. *Mod Pathol* 2014; 27: 472–491.
- 780 [9] Sumazin P, Peters TL, Sarabia SF, et al. Hepatoblastomas with carcinoma features
781 represent a biological spectrum of aggressive neoplasms in children and young adults. *J*
782 *Hepatol* 2022; 77: 1026–1037.
- 783 [10] Eichenmüller M, Trippel F, Kreuder M, et al. The genomic landscape of hepatoblastoma
784 and their progenies with HCC-like features. *J Hepatol* 2014; 61: 1312–1320.
- 785 [11] Gröbner SN, Worst BC, Weischenfeldt J, et al. The landscape of genomic alterations
786 across childhood cancers. *Nature* 2018; 555: 321–327.
- 787 [12] Koch A, Denkhaus D, Albrecht S, et al. Childhood hepatoblastomas frequently carry a
788 mutated degradation targeting box of the beta-catenin gene. *Cancer Res* 1999; 59: 269–
789 73.
- 790 [13] Cairo S. Activation of Wnt and Myc signaling in hepatoblastoma. *Frontiers in Bioscience*
791 2012; E4: 480.
- 792 [14] Honda S, Arai Y, Haruta M, et al. Loss of imprinting of IGF2 correlates with
793 hypermethylation of the H19 differentially methylated region in hepatoblastoma. *Br J*
794 *Cancer* 2008; 99: 1891–1899.

- 795 [15] Hirsch TZ, Pilet J, Morcrette G, et al. Integrated Genomic Analysis Identifies Driver
796 Genes and Cisplatin-Resistant Progenitor Phenotype in Pediatric Liver Cancer. *Cancer*
797 *Discov* 2021; 11: 2524–2543.
- 798 [16] Breuhahn K, Longerich T, Schirmacher P. Dysregulation of growth factor signaling in
799 human hepatocellular carcinoma. *Oncogene* 2006; 25: 3787–800.
- 800 [17] Tovar V, Alsinet C, Villanueva A, et al. IGF activation in a molecular subclass of
801 hepatocellular carcinoma and pre-clinical efficacy of IGF-1R blockage. *J Hepatol* 2010;
802 52: 550–559.
- 803 [18] Martinez-Quetglas I, Pinyol R, Dauch D, et al. IGF2 Is Up-regulated by Epigenetic
804 Mechanisms in Hepatocellular Carcinomas and Is an Actionable Oncogene Product in
805 Experimental Models. *Gastroenterology* 2016; 151: 1192–1205.
- 806 [19] World Health Organization. International Nonproprietary Names for Pharmaceutical
807 Substances (INN) RECOMMENDED International Nonproprietary Names: List 76. *WHO*
808 *Drug Information* 2016; 30: 477–544.
- 809 [20] de Bono J, Lin C-C, Chen L-T, et al. Two first-in-human studies of xentuzumab, a
810 humanised insulin-like growth factor (IGF)-neutralising antibody, in patients with
811 advanced solid tumours. *Br J Cancer* 2020; 122: 1324–1332.
- 812 [21] Carrillo-Reixach J, Torrens L, Simon-Coma M, et al. Epigenetic footprint enables
813 molecular risk stratification of hepatoblastoma with clinical implications. *J Hepatol*
814 2020; 73: 328–341.
- 815 [22] Perilongo G, Maibach R, Shafford E, et al. Cisplatin versus cisplatin plus doxorubicin for
816 standard-risk hepatoblastoma. *N Engl J Med* 2009; 361: 1662–70.
- 817 [23] Hooks KB, Audoux J, Fazli H, et al. New insights into diagnosis and therapeutic options
818 for proliferative hepatoblastoma. *Hepatology* 2018; 68: 89–102.
- 819 [24] Robinson MD, McCarthy DJ, Smyth GK. edgeR: a Bioconductor package for differential
820 expression analysis of digital gene expression data. *Bioinformatics* 2010; 26: 139–140.
- 821 [25] Langfelder P, Horvath S. WGCNA: an R package for weighted correlation network
822 analysis. *BMC Bioinformatics* 2008; 9: 559.
- 823 [26] Ashburner M, Ball CA, Blake JA, et al. Gene Ontology: tool for the unification of biology.
824 *Nat Genet* 2000; 25: 25–29.
- 825 [27] Borad MJ, Champion MD, Egan JB, et al. Integrated genomic characterization reveals
826 novel, therapeutically relevant drug targets in FGFR and EGFR pathways in sporadic
827 intrahepatic cholangiocarcinoma. *PLoS Genet* 2014; 10: e1004135.
- 828 [28] Xie C, Leung Y-K, Chen A, et al. Differential methylation values in differential
829 methylation analysis. *Bioinformatics* 2019; 35: 1094.
- 830 [29] Piskol R, Ramaswami G, Li JB. Reliable Identification of Genomic Variants from RNA-Seq
831 Data. *The American Journal of Human Genetics* 2013; 93: 641–651.
- 832 [30] Cibulskis K, Lawrence MS, Carter SL, et al. Sensitive detection of somatic point
833 mutations in impure and heterogeneous cancer samples. *Nature Biotechnology* 2013
834 31:3 2013; 31: 213–219.

- 835 [31] Nicolle D, Fabre M, Simon-Coma M, et al. Patient-derived mouse xenografts from
836 pediatric liver cancer predict tumor recurrence and advise clinical management.
837 *Hepatology* 2016; 64: 1121–1135.
- 838 [32] Broutier L, Mastrogianni G, Verstegen MM, et al. Human primary liver cancer–
839 derived organoid cultures for disease modeling and drug screening. *Nat Med* 2017; 23:
840 1424–1435.
- 841 [33] Hartmann W, Waha A, Koch A, et al. p57(KIP2) is not mutated in hepatoblastoma but
842 shows increased transcriptional activity in a comparative analysis of the three imprinted
843 genes p57(KIP2), IGF2, and H19. *Am J Pathol* 2000; 157: 1393–1403.
- 844 [34] Cairo S, Armengol C, de Reyniès A, et al. Hepatic Stem-like Phenotype and Interplay of
845 Wnt/ β -Catenin and Myc Signaling in Aggressive Childhood Liver Cancer. *Cancer Cell*
846 2008; 14: 471–484.
- 847 [35] Chiang DY, Villanueva A, Hoshida Y, et al. Focal gains of VEGFA and molecular
848 classification of hepatocellular carcinoma. *Cancer Res* 2008; 68: 6779–88.
- 849 [36] Vu TH, Hoffman AR. Promoter-specific imprinting of the human insulin-like growth
850 factor-II gene. *Nature* 1994; 371: 714–7.
- 851 [37] Bell AC, Felsenfeld G. Methylation of a CTCF-dependent boundary controls imprinted
852 expression of the Igf2 gene. *Nature* 2000; 405: 482–485.
- 853 [38] Li X, Cui H, Sandstedt B, et al. Expression levels of the insulin-like growth factor-II gene
854 (IGF2) in the human liver: developmental relationships of the four promoters. *Journal of*
855 *Endocrinology* 1996; 149: 117–124.
- 856 [39] Liu M, Roth A, Yu M, et al. The IGF2 intronic miR-483 selectively enhances transcription
857 from IGF2 fetal promoters and enhances tumorigenesis. *Genes Dev* 2013; 27: 2543–
858 2548.
- 859 [40] Ramer R, Schmied T, Wagner C, et al. The antiangiogenic action of cisplatin on
860 endothelial cells is mediated through the release of tissue inhibitor of matrix
861 metalloproteinases-1 from lung cancer cells. *Oncotarget* 2018; 9: 34038–34055.
- 862 [41] Nagae G, Yamamoto S, Fujita M, et al. Genetic and epigenetic basis of hepatoblastoma
863 diversity. 2021; 12: 5423.
- 864 [42] Gray SG, Eriksson T, Ekström C, et al. Altered expression of members of the IGF-axis in
865 hepatoblastomas. *Br J Cancer* 2000; 82: 1561–1567.
- 866 [43] Venkatraman A, He XC, Thorvaldsen JL, et al. Maternal imprinting at the H19-Igf2 locus
867 maintains adult haematopoietic stem cell quiescence. *Nature* 2013; 500: 345–9.
- 868 [44] Pollak M. The insulin and insulin-like growth factor receptor family in neoplasia: an
869 update. *Nat Rev Cancer* 2012; 12: 159–169.
- 870 [45] Bergman D, Halje M, Nordin M, et al. Insulin-like growth factor 2 in development and
871 disease: a mini-review. *Gerontology* 2013; 59: 240–9.
- 872 [46] Li X, Nong Z, Ekström C, et al. Disrupted IGF2 promoter control by silencing of promoter
873 P1 in human hepatocellular carcinoma. *Cancer Res* 1997; 57: 2048–54.

- 874 [47] Rovina D, La Vecchia M, Cortesi A, et al. Profound alterations of the chromatin
875 architecture at chromosome 11p15.5 in cells from Beckwith-Wiedemann and Silver-
876 Russell syndromes patients. *Sci Rep* 2020; 10: 8275.
- 877 [48] Li X, Nadauld L, Ootani A, et al. Oncogenic transformation of diverse gastrointestinal
878 tissues in primary organoid culture. *Nat Med* 2014; 20: 769–77.
- 879 [49] Belharazem D, Magdeburg J, Berton AK, et al. Carcinoma of the colon and rectum with
880 deregulation of insulin-like growth factor 2 signaling: clinical and molecular
881 implications. *J Gastroenterol* 2016; 51: 971–984.
- 882 [50] Lee H, Kim N, Yoo YJ, et al. β -catenin/TCF activity regulates IGF-1R tyrosine kinase
883 inhibitor sensitivity in colon cancer. *Oncogene* 2018; 37: 5466–5475.
- 884 [51] Friedbichler K, Hofmann MH, Kroeze M, et al. Pharmacodynamic and Antineoplastic
885 Activity of BI 836845, a Fully Human IGF Ligand-Neutralizing Antibody, and Mechanistic
886 Rationale for Combination with Rapamycin. *Mol Cancer Ther* 2014; 13: 399–409.
- 887 [52] Sivaprakasam P, Gupta AA, Greenberg ML, et al. Survival and long-term outcomes in
888 children with hepatoblastoma treated with continuous infusion of cisplatin and
889 doxorubicin. *J Pediatr Hematol Oncol* 2011; 33: e226–e230.
- 890 [53] Wei M, Yuan X. Cisplatin-induced Ototoxicity in Children With Solid Tumor. *J Pediatr*
891 *Hematol Oncol* 2019; 41: E97–E100.
- 892 [54] Ferte C, Loriot Y, Clémenson C, et al. IGF-1R targeting increases the antitumor effects of
893 DNA-damaging agents in SCLC model: An opportunity to increase the efficacy of
894 standard therapy. *Mol Cancer Ther* 2013; 12: 1213–1222.
- 895 [55] Yao N, Yao D, Wang L, et al. Inhibition of autocrine IGF-II on effect of human HepG2 cell
896 proliferation and angiogenesis factor expression. *Tumor Biology* 2012; 33: 1767–76.
- 897
- 898

899 TABLES

	IGF2 ^{high} (n = 22)	IGF2 ^{low} (n = 9)	p value
Age (months), median (range)	17.5 (1-180)	13 (3-63)	0.71
>3 years, n (%)	6 (27%)	3 (33%)	1
Gender (male), n (%)	13 (59%)	6 (67%)	1
Serum AFP, ng/mL (range)	620,000 (341- 2,000,000)	160,000 (663- 2,186,461)	0.27
>1000 ng/ml, n (%)	20 (95%)	7 (78%)	0.21
>1,000,000 ng/ml, n (%)	5 (23%)	1 (11%)	0.64
CHIC* classification (High risk), n (%)	9 (41%)	2 (22%)	0.43
PRETEXT classification			
PRETEXT I	0 (0%)	2 (22%)	0.08
PRETEXT II	9 (41%)	2 (22%)	0.43
PRETEXT III	8 (36%)	4 (44%)	0.70
PRETEXT IV	5 (23%)	1 (11%)	0.64
Neo-adjuvant chemotherapy, n (%)	21 (95%)	9 (100%)	1
Distant metastasis at diagnosis, n (%)	7 (32%)	2 (22%)	0.69
Vascular invasion, n (%)	10 (45%)	2 (22%)	0.42
Multifocality	10 (45%)	1 (11%)	0.11
HCN-NOS [§] , n (%)	2 (9%)	0	1
SCUD [#] , n (%)	3 (13%)	1 (11%)	1
Tumor histology			
Epithelial, n (%)	12 (55%)	3 (33%)	0.43
Mixed epithelial and mesenchymal, n (%)	10 (45%)	6 (97%)	0.43
Main Epithelial Component			
Fetal, n (%)	8/22 (36%)	5 (56%)	0.43
Non-Fetal, n (%)	9/22 (41%)	1 (11%)	0.20

900 **Table 1.** Clinico-pathological features of patients with IGF2-high and -low HB in the study
 901 cohort (n=31). *CHIC, Children's Hepatic Tumors International Collaboration-Hepatoblastoma
 902 Stratification (CHIC-HS). [§]HCN-NOS: Hepatocellular Malignant Neoplasm, Not Otherwise
 903 Specified. [#]SCUD: Small cell undifferentiated hepatoblastoma.

904

905 FIGURE LEGENDS

906 **Figure 1. Characterization of IGF2^{high} HB tumors. (A)** *IGF2* expression levels
 907 determined by quantitative RT-PCR in healthy liver, adjacent non-tumoral liver tissue
 908 and HB tumor samples (left). HB tumor samples classified as IGF2^{high} and IGF2^{low}
 909 (right). *p < 0.05, **p < 0.01, ***p < 0.001. **(B)** Molecular profile of IGF2^{high} and IGF2^{low}
 910 HB tumors. *IGF2* expression levels were determined by RNA-seq and qRT-PCR. IGF2^{high}
 911 was defined as fold-change (FC) > 4 *versus* mean adjacent non-tumoral tissue for qRT-
 912 PCR; and as FC > 2 *versus* median adjacent non-tumoral tissue for RNA-seq. The dashed
 913 red line marks the age of 3 years. HB: hepatoblastoma. HCN-NOS: Hepatocellular
 914 Malignant Neoplasm, Not Otherwise Specified. Statistical tests: t test and Fisher.
 915 Displayed p values were obtained comparing IGF2^{high} and IGF2^{low} HBs. **(C)** Kaplan-
 916 Meier's plots for recurrence-free survival of IGF2^{high} (n=9) and IGF2^{low} (n=22) HB
 917 patients. Statistical test: log Rank.

918 **Figure 2. Epigenetic deregulations in IGF2^{high} HB tumors. (A)** Methylation levels in
 919 CpGs located within the *IGF2* adult promoter (P1), fetal promoters (P2-P4), and ICR1
 920 regulatory region of adjacent (n = 22), IGF2^{high} tumors (n = 18) and IGF2^{low} tumors (n =
 921 9). Error bars indicate mean ± standard deviation (SD). **(B)** Human Transcriptome Array
 922 (HTA) data showing the expression of adult and fetal specific exons of *IGF2* between
 923 IGF2^{high} (red, n = 22) and IGF2^{low} (blue, n = 9) tumors. The coding exons of the *IGF2*
 924 gene are shown below the plot. The specific exons of the adult (hg19, chr 11:
 925 2,170,833-2,170,356 and 2,169,037-2,168,796) and fetal (2,160,619-2,159,459) *IGF2*
 926 isoforms are shown in green and red, respectively. The common coding exons in adult
 927 and fetal *IGF2* isoforms are shown in gray. The gray shadow in the plot indicates no
 928 gene expression (values below the baseline level). **(C)** Expression levels of fetal P3-
 929 derived and adult P1-derived *IGF2* isoforms determined by quantitative RT-PCR in
 930 healthy livers (n=5), adjacent liver tissue (n=25), and in IGF2^{high} (n=17) and IGF2^{low}
 931 (n=8) HB tumor samples. **(D)** Allelic imbalances in HB determined using CystoScan SNP
 932 array data. Chromosomal regions with loss of heterozygosity in HB tumors are shown
 933 in red, and the frequency of each alteration, in grey. **(E)** Frequency of LOH in 11p15.5
 934 in IGF2^{high} (n = 21) and IGF2^{low} HB (n = 9) samples. **(F)** MiR-483-5p expression levels in
 935 IGF2^{high} and IGF2^{low} HB samples assessed by quantitative RT-PCR (left) and RNA

sequencing (right). * $P < 0.05$, ** $P < 0.01$, *** $P < 0.001$ in IGF2^{high} vs IGF2^{low} unless otherwise indicated; # $P < 0.05$, ## $P < 0.01$, ### $P < 0.001$ in IGF2^{high} vs Adjacent.

938

Figure 3. Integrated mechanisms of IGF2 overexpression in HB tumors. Heatmap presenting the epigenetic and genomic deregulations affecting each HB tumor. Fetal promoter hypomethylation occurred in 50% of IGF2^{high} cases; ICR1 gain of methylation in 61% IGF2-related allelic imbalances, in 57% of IGF2^{high} cases; and miR483 overexpression, in 55% of IGF2^{high} cases. Statistical significance between IGF2^{high} and IGF2^{low} was calculated by Fisher and t tests.

945

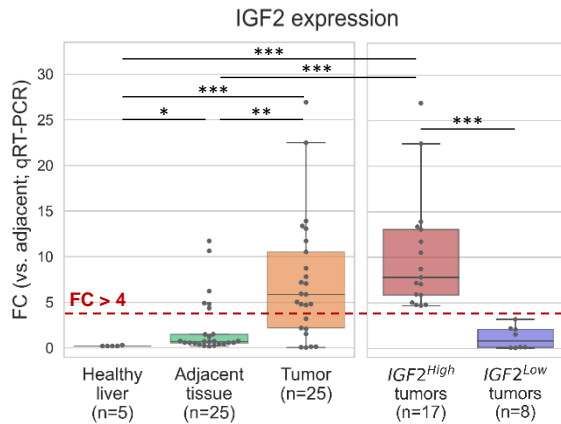
Figure 4. Anti-proliferative and pro-apoptotic effect of IGF2 inhibition in combination with cisplatin in HB cell lines and organoids. (A-B) Cell viability **(A)** and colony formation capacity **(B)** in HepG2 and Huh6 cell lines treated with increasing concentrations of cisplatin and xentuzumab **(A)** or with cisplatin (0.3 μ M), xentuzumab (1 μ M) or its combination (combo) **(B)**. **(C)** Cell viability in IGF2^{high} tumor organoids treated with increasing concentrations of cisplatin (0-10 μ M) and xentuzumab (0-100 nM). **(D)** IC₅₀ curves for cisplatin alone (left) and cisplatin combined with xentuzumab (right). IC₅₀ values for cisplatin are indicated. **(E)** Caspase C3-dependent apoptosis analysis in tumor organoids treated with growing concentrations of cisplatin (0-5 μ M) and xentuzumab (0-100 nM). Error bars indicate mean \pm standard deviation (SD). **(F)** Representative Western blot analysis and quantification of the IGF2/IGF1R pathway in tumor organoids stimulated by IGF2 and treated with xentuzumab and/or cisplatin. Histone H3 was used as a loading control. * $P < 0.05$, ** $P < 0.01$.

Figure 5. Antitumor effect of xentuzumab plus cisplatin in an IGF2^{high} xenograft model. (A) Survival, measured as time to reach 1500 mm³, in animals treated with control IgG (n = 14), cisplatin (n = 13), xentuzumab (n = 14) or its combination (n = 14). **(B)** Representative images of H&E slides in mice treated with control IgG, cisplatin, xentuzumab or its combination. Images were captured at 40x. **(C)** Representative H&E stainings for each treatment regimen. **(D)** CD31 staining in tumors from treated mice.

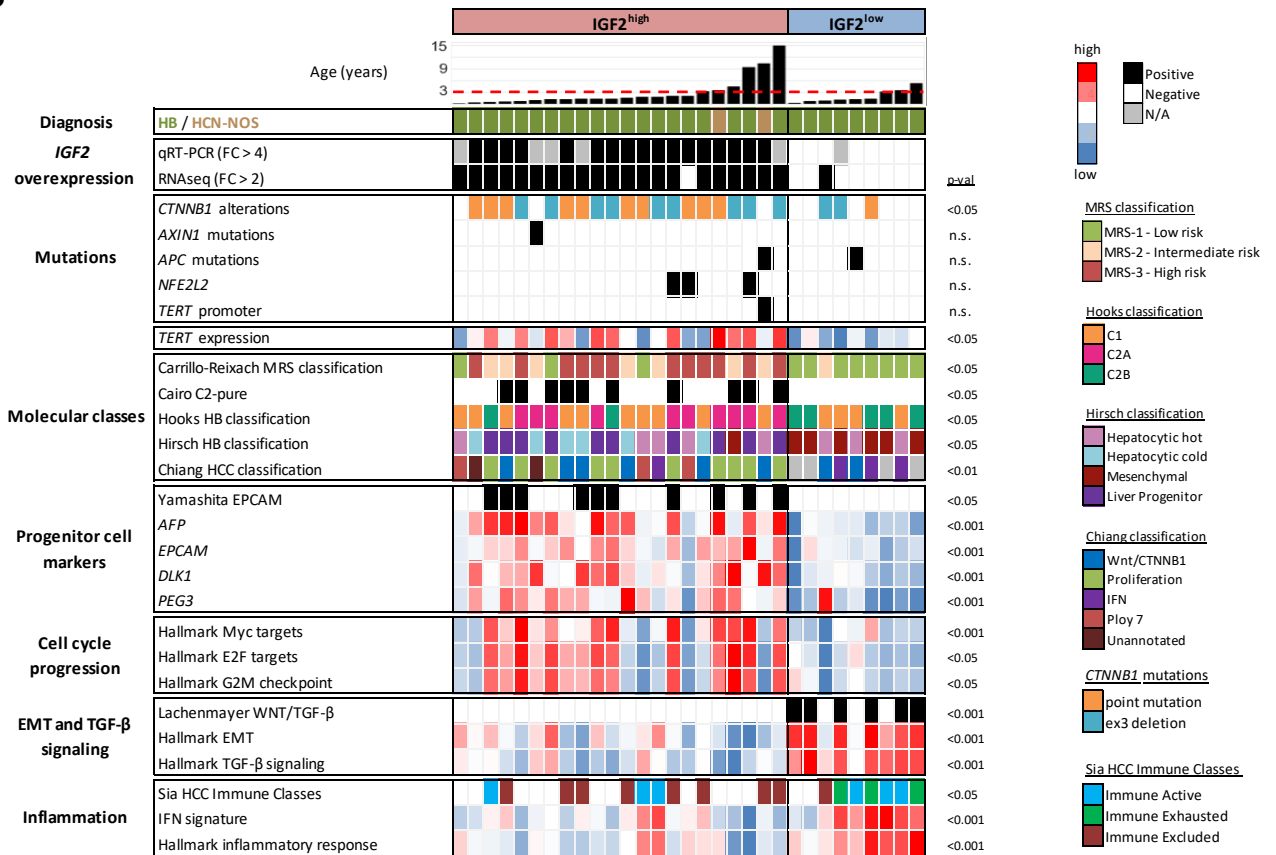
965 Error bars indicate mean \pm standard deviation (SD). * $P < 0.05$; ** $P < 0.01$, *** $P <$
966 0.001.

Figure 1

A



B



C

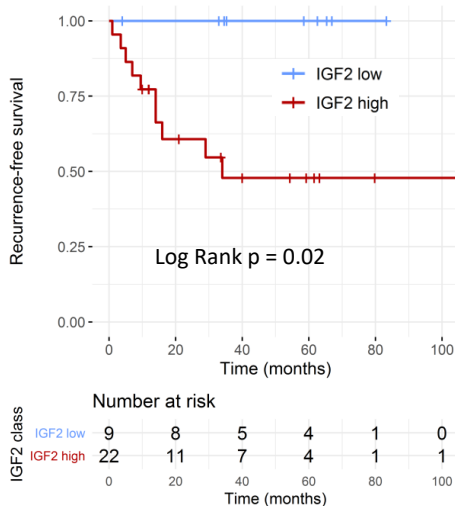
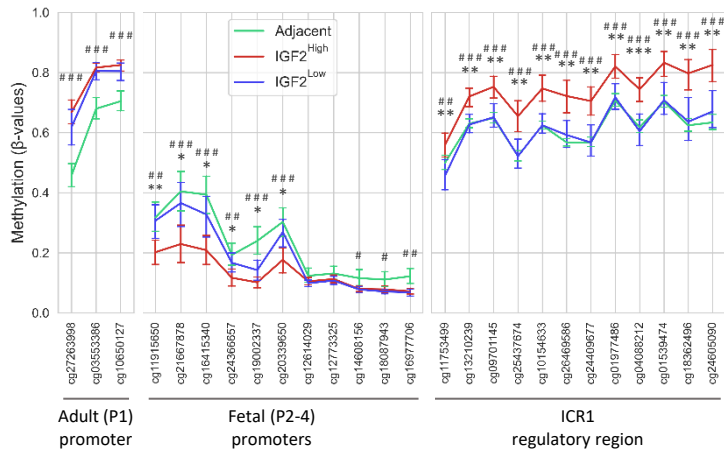
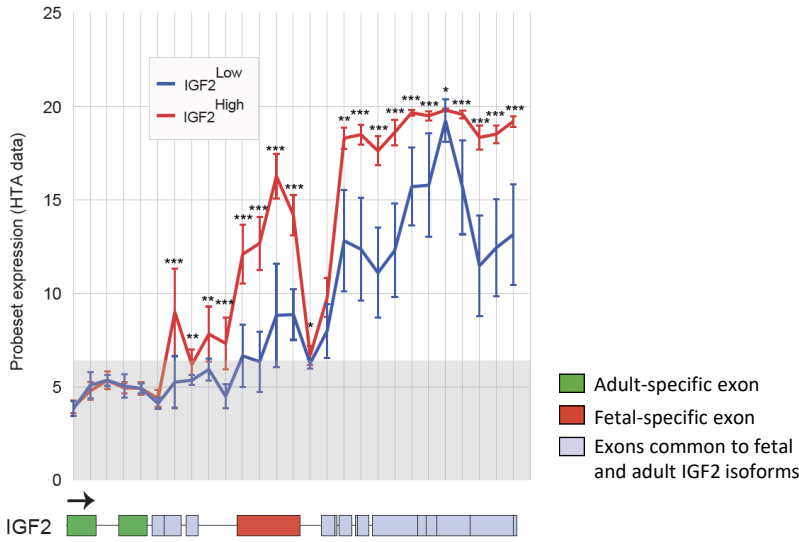


Figure 2

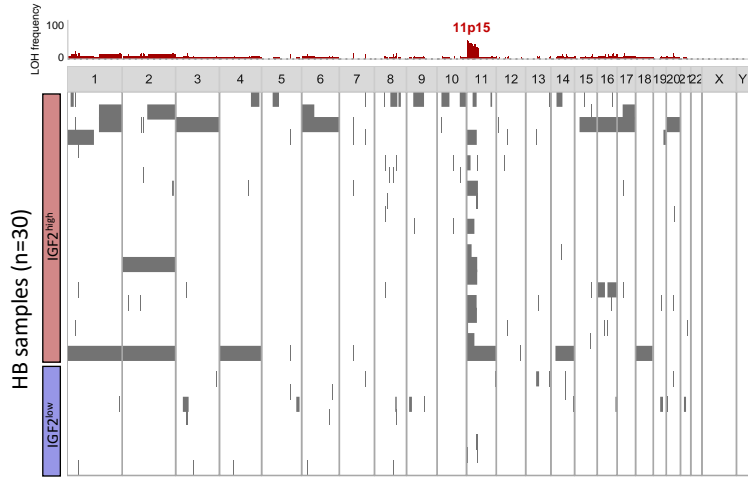
A



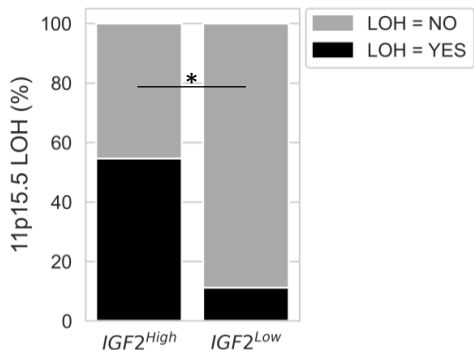
B



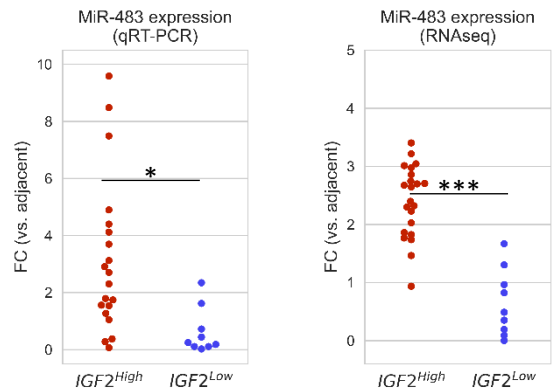
D



E



F



C

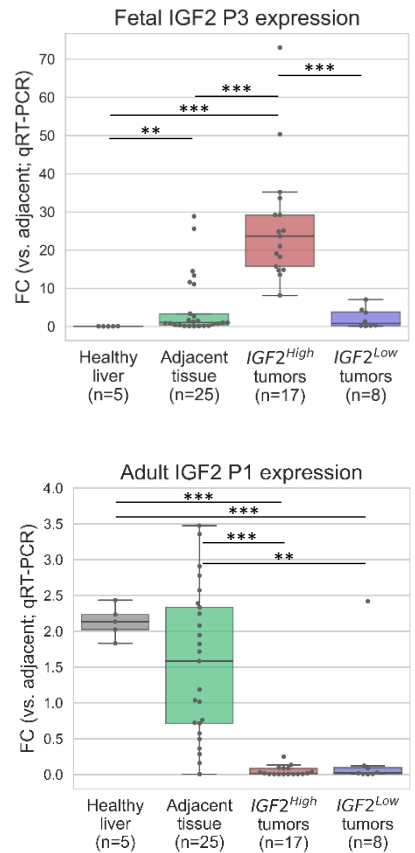


Figure 3

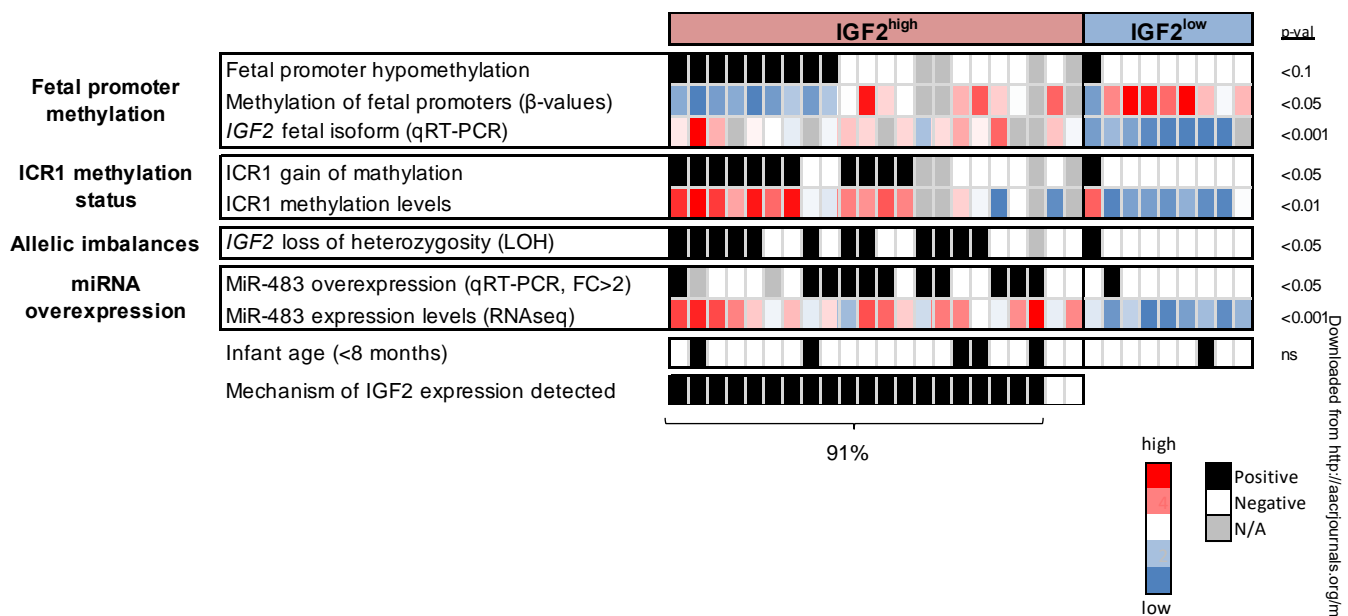
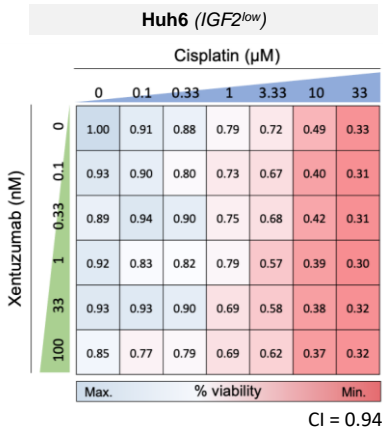
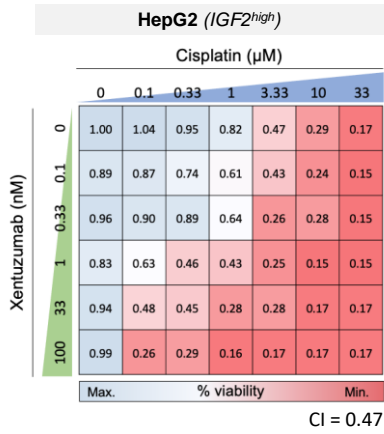
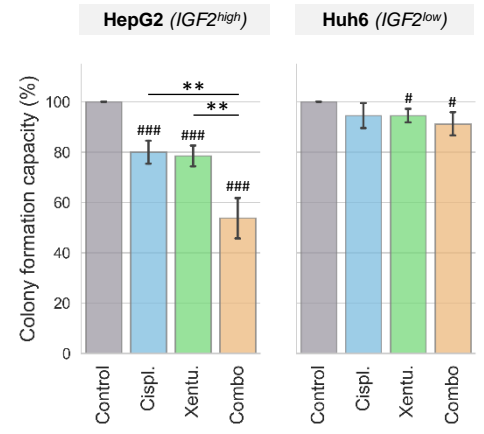


Figure 4

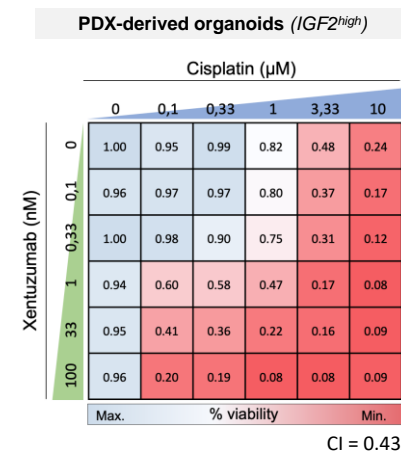
A



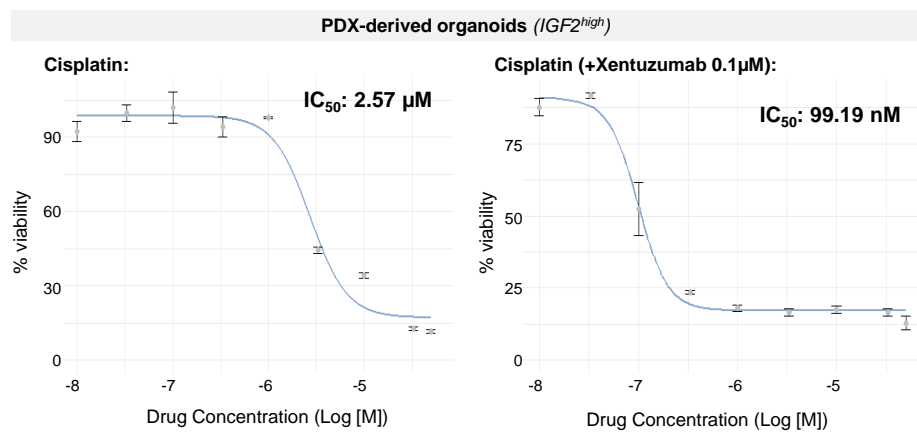
B



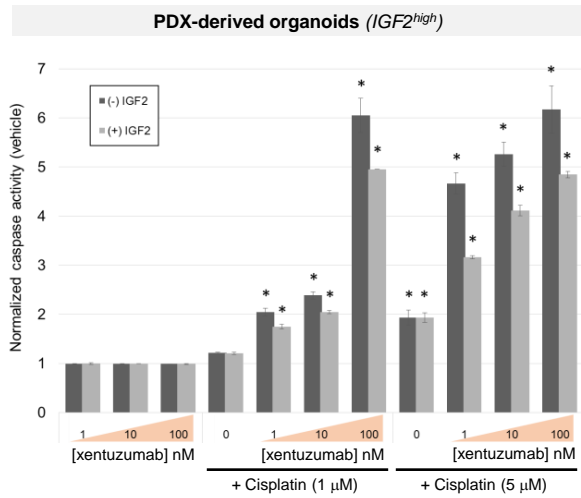
C



D



E



F

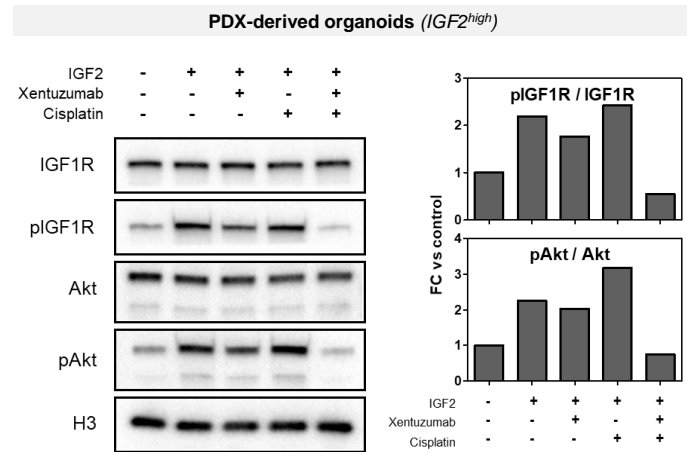
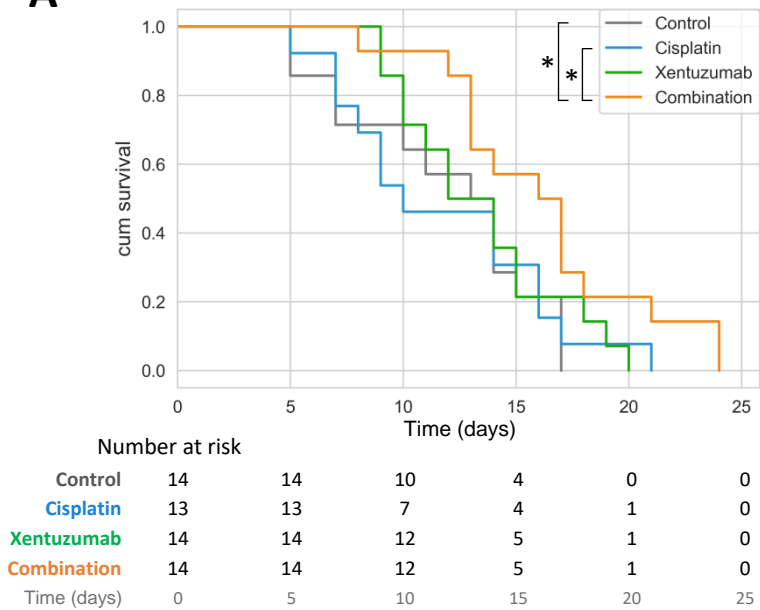
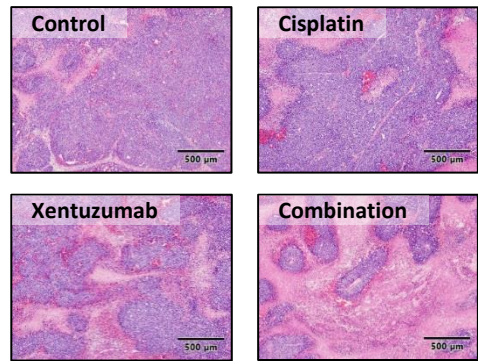


Figure 5

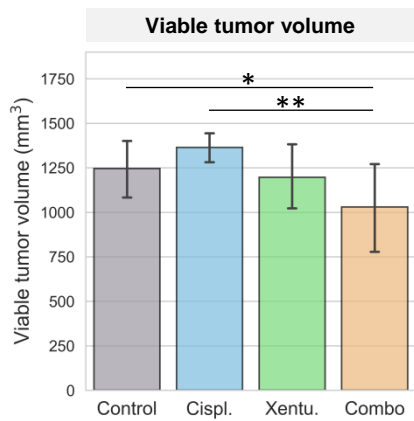
A



B



C



D

